PROSIDING SNTTM XXIII 2025
Volume 23, No. 1, Tahun 2025, 9 Oktober 2025
e-ISSN 2623-0313
p-ISSN 3032-1972

Process modelling of friction stir welding of AA1100 Aluminum alloy using a hexagon-shaped tool to optimize the process parameters

Indrawanto[a,1], Luon Virak[b], Tri Prakosa[a], Agung Wibowo[a], Sri Raharno[a], Indria Herman[a], Vani Virdyawan[a]
[a]Program Studi Teknik Mesin, Fakultas Teknik Mesin dan Dirgantara, Institut Teknologi Bandung, Bandung 40132
[b]Program Magister Teknik Mesin, Institut Teknologi Bandung, Bandung 40132
[1]Email korespondensi: indrawanto@itb.ac.id

Abstract. This paper presents process modeling of Friction Stir Welding (FSW) to optimize the mechanical properties of friction-stir-welded 1100 Aluminum alloy. The model variables are the tool rotational speed, the translational feed rate, and the axial force. The model is developed using a statistical engineering method known as Response Surface Methodology (RSM). Analysis of variance techniques have been used to assess the adequacy of the model. The effects of welding parameters on the mechanical properties, macrostructure, and microstructure of friction-stir-welded joints have been analyzed in detail, and the predicted trends are discussed. The developed mathematical model can predict the tensile strength of friction-stir-welded AA1100 Aluminum alloy joints with 95% confidence.

Keywords: Friction Stir Welding; Aluminum alloy; Mechanical properties; Tensile strength; Rotational speed; Welding speed; Axial force; Macro and micro-structure.

Received: 30 September 2025; **Presented:** 9 October 2025; **Publication:** 9 March 2026
DOI: https://doi.org/10.71452/pkq5rh02

INTRODUCTION

Friction Stir Welding (FSW) is considered a solid-state joining technique that uses a combination of friction and plastic deformation, driven by a rotating shoulder and pin, to weld sheet materials. It was invented by Wayne Thomas and his colleagues at The Welding Institute (TWI) in Cambridge, United Kingdom. Later, FSW was initially filed into a British patent in the United Kingdom under the name of "Improvements of Friction Welding" in December 1991 [1].

Over a short period, FSW demonstrated significant potential to produce high-quality welds in various materials. The capital investment in FSW can be significantly reduced by adapting milling machines to perform the process. Currently, the FSW technique has been successfully applied to manufacture space shuttle fuel tanks, aluminum decking for car ferries, compound aluminum extrusions, and automotive structural components. Although several facilities have reported experiments on lead, magnesium, copper, titanium, and steel, most of the applications are performed in aluminum industries, which are difficult to join by the fusion welding process [2]. FSW may also be used for the joining process of polymer materials [3]. The FSW has numerous advantages over traditional welding methods, including improved mechanical properties, improved joint integrity, and environmental impact [4], [5], [6], [7].

The RSM method has been used to predict the properties of some friction stir-welded aluminum alloys. Rajakumar et al. established empirical relationships to predict grain size, ultimate tensile strength, hardness, and corrosion rate of friction stir-welded AA 1100 and AA 6061-T6 aluminum alloy joints using RSM [8]. Heidarzadeh et al. used the RSM method to create mathematical models predicting the ultimate tensile strength and elongation of the AA 6061-T4 aluminum alloys [9]. Rose et al. used RSM to predict and optimize the pulsed current tungsten inert gas welding parameters to attain maximum tensile strength in AZ61A magnesium alloy [10]. Paventhan et al. also used RSM to predict and optimize the tensile strength of friction welding parameters for joining aluminum alloy and stainless steel [11]. De Filipis et al. applied RSM to optimize the FSW sheets AA 5754-H111[12].

Although many researchers have used the RSM method to develop the mechanical properties of various alloys, an investigation into the development of mathematical relationships between mechanical properties and welding parameters for friction-stir-welded AA1100 is still lacking. Therefore, the objective of this research is to establish the functional relationships between three operating variables of FSW, including tool rotational speed, welding speed, and tool axial forces, and tensile strength (TS) of friction stir-welded AA1100 aluminum alloy joints using the RSM method in conjunction with the central composite rotatable design (CCRD). These relationships can then be used to predict mechanical properties and determine optimal operating parameters.

This paper is organized as follows: this section presents an introduction to FSW and the research purpose. Section 2 presents the principle of FSW and its parameters. Section 3 presents the experimental procedures of FSW. Section 4 presents experimental

e-ISSN 2623-0313
p-ISSN 3032-1972

results and analysis. Section 5 presents mathematical modeling to optimize the FSW process. Section 6 presents macro- and microstructural investigations to determine the relationship between macro- and microstructures and the tensile strength of FSW. Section 7 presents the optimized FSW parameters, and Section 8 presents the conclusion of this paper.

FSW PROCESS PRINCIPLES

FSW has been identified and termed as a thermo-mechanical [13] and the hot working deformation process [14]. This process relies on both thermal and material flow to initiate softening and displacement of a finite volume of workpiece material, i.e., material in the direct vicinity of the joining tool. During the process, a non-consumable rotating tool with a specially designed pin and shoulder is inserted into the abutting edges of sheets or plates to be joined and subsequently traversed along the joint line, as shown in Figure 1. As the FSW tool rotates in the counterclockwise direction, the advancing side is on the left, where the tool rotation direction is the same as the tool travel direction, and the retreating side is on the right, where the tool rotation is opposite the tool travel direction. FSW joining is the result of an interaction between three principal processing parameters, namely tool rotation speed, weld travel speed, and axial forces. Forces generated during the FSW process act in three-dimensional spaces. The force along the X-axis, Y-axis, and Z-axis will be referred to as the translational (FX), transverse (FY), and axial force (FY), respectively [15].

FSW investigations show that the stir zone will decrease in size rather than increase with ever-increasing tool rotation speed [16]. It is well acknowledged that process temperatures during FSW are influenced by process parameters, while material properties of the workpiece, the tool, and clamping/backing system, will affect process temperature profiles through cooling rates, and that these relationships will ultimately determine the mechanical properties of the friction stir welded joint [17]. It is well accepted that peak process temperature increases with increasing tool rotation or decreasing weld travel speed. Macrographs, micrographs, Transmission Electron Microscopy (TEM), microhardness measurements, and mechanical destructive testing of the weld are typical bases for investigating friction stir welds. It has also been reported that the rotation speed of the FSW tool has substantially greater influence on the microstructure and mechanical properties of friction stir welds than either the influence of weld travel speed or axial force [18]. It should be noted that in terms of mechanical properties, both the yield strength and ultimate tensile strength of the welded joint approached 96% that achieved in the base material, while the rupture elongation measured almost 70% against the base material. The key to successfully FSW high-strength precipitation hardening aluminum alloys is to maintain the working temperature as high as possible as close to the solidus, though accurate melting or localized/incipient melting should be avoided [16].
Microstructural zones in FSW joint are divided into four distinct regions shown in Figure 2, and the regions will be described as follows [15]. Base Metal (BM) is the region which is not affected by the thermo cycle of the FSW process although it is close to the heat-affected zone. The material in BM region is observed to have the same properties as those of base material. The Heat-Affected Zone (HAZ) is located closer to the weld center and is heated sufficiently during welding to alter its properties without plastic deformation of the original grain structure. Changes in the HAZ may include variations in the workpiece's strength, ductility, corrosion susceptibility, and toughness. The Thermo-Mechanically Affected Zone (TMAZ) encompasses all plastically deformed material within the joint region. The FSW workpiece is sufficiently heated and softened, and the process forces are sufficiently high to result in plastic deformation of the original grain structure without recrystallization in this region.

The Weld Nugget (WN) is the fully recrystallized area, or the stir zone, previously occupied by the tool pin. The term stir zone is commonly used in friction stir processing, where large volumes of material are processed. To avoid the tool pin from contacting the backing plate, the tool shoulder is plunged into the FSW workpiece to a predetermined depth, typically 0.1-0.2 mm. The pin is designed to be slightly shorter than the workpiece thickness, with a diameter approximately equal to or slightly larger than the workpiece thickness. Normally, the pin length is kept as close as possible to the weld root, especially for full-penetration butt welds.

The FSW welding tool can be tilted. Depending on the tool shoulder design, the tool angle is typically tilted up to 4 degrees. The tool tilt angle affects material flow around the tool pin and under the tool shoulder, helping consolidate the material behind the tool but limiting welding speed. Tool tilt can cause the tool to lift off the material if the tilt angle is too high during welding. An increase in tilt angles will increase material displacement, causing the material to flash out and the vertical force on the tool to increase [15].

The required fixture design is essential for rigidly fixing the plates to be joined in a welding fixture, as shown in Figure 3.

The process requires the workpieces to be prevented from spreading or lifting during welding. So, welding fixtures are typically equipped with features

e-ISSN 2623-0313
p-ISSN 3032-1972

that restrain the workpiece. FSW fixtures are equipped with a removable anvil insert that can be replaced if the anvil is inadvertently damaged by contact with the welding tool pin. Since the anvil insert is closely coupled to the workpiece at the weld point, it is important to consider its heat capacity and diffusivity when designing FSW fixtures to manage heat transfer properly. The selection of anvil or baking plate material also significantly affects the FSW process, and great care must be taken to select a material with the desired thermal conductivity (Table 1).

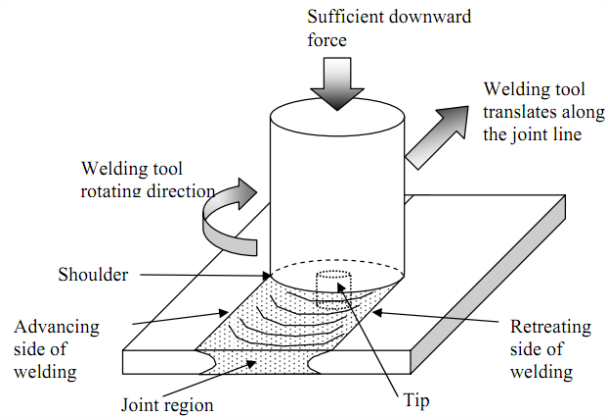

Figure 1. Friction Stir Welding process

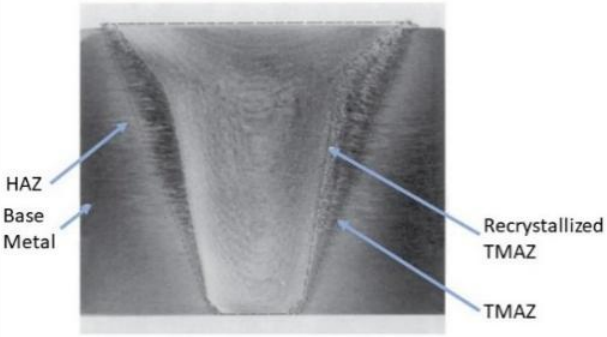

Figure 2. Macro-structural zone in the FSW joint [2].

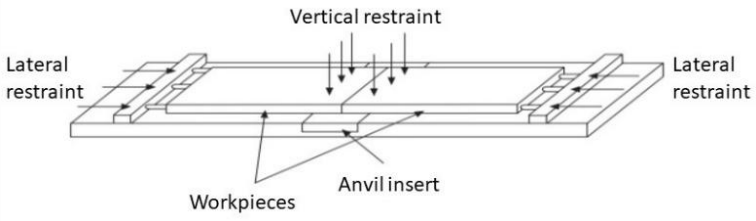

Figure 3. FSW fixture requirements [2]

Table 1. Thermal Conductivity for backing plates [2]

Material	**Thermal Conductivity [W/m.K]**
Mild steel	40-60
Stainless steel	15-25
X33CrS16	17
RAMAX	24
Bras	110-150
Copper	380-400
Aluminum alloys	110-235

e-ISSN 2623-0313
p-ISSN 3032-1972

EXPERIMENTAL PROCEDURES

AA1100 aluminum alloy is a low-strength commercial grade aluminum alloy, which is used in chemical process plant equipment, pyrotechnic powder, architectural flashings, lamp reflectors, and cable sheathing. The nominal thickness of the AA1100 plate is 2.65 mm, and the ultimate tensile strength is 110 MPa. The nominal compositions and mechanical properties of AA1100 are shown in Tables 2 and 3, respectively.

WELDING TOOL DESIGN

The FSW welding tool is considered as the heart of the welding process. The adequacy of the designed tool features and the selection of the tool material are key factors in generating sufficient heat to stir the workpiece to be welded, which strongly affects the mechanical properties of the welded aluminum plate. For this reason, a welding tool consisting of a cylindrical shoulder and an octagonal-shaped pin has been designed for the FSW welding process. The tool's designed feature is shown in Figure 4.

High-speed steel tool (HSS-M2) was selected as the welding tool material. The chemical compositions and heat treatment temperatures of the HSS-M2 are shown in Tables 4 and 5, respectively.

Table 2. The chemical composition of AA1100 parent metal (wt.%) [19]

Alloy	Mg	Mn	Si	Fe	Cu	Ti	Zn	Al
AA110	0.152	0.508	0.004	0.061	0.0015	0.0016	0.0006	Balance

Table 3. Mechanical properties of AA 1100 parent material [19]

Alloy	Yield Strength	Tensile Strength	Hardness	Elongation
AA1100	95 MPa	110 MPa	70 HV	5 mm (in 50 mm)

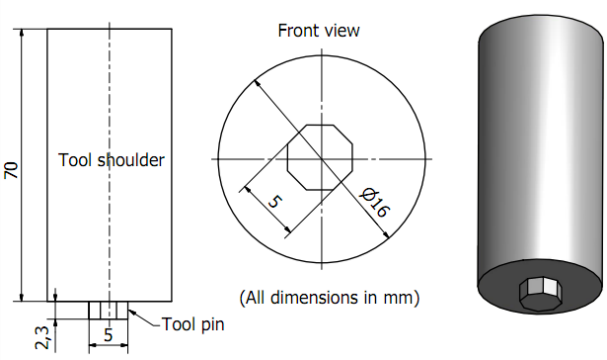

Figure 4. FSW welding tool and its dimensions

Table 4. Chemical composition of HSS (weight%) [20]

Alloy	P	S	V	Mn	Si	Cr	C	W	Mo
HSS-M2	0.03	0.03	1.75-1.20	0.15-1.40	0.20-0.45	3.75-4.50	0.78-0.88	5.50-6.75	4.50-5.50

Table 5. Heat treatment temperature of HSS material [20]

Alloy	Preheat temperature (^{0}C)	Austenitizing Temperature (^{0}C)	Tempering Temperature (^{0}C)	Minimum Hardness (Rockwell C)
HSS-M2	732-843	1216	552	64

In this study, a CNC milling machine, MAHO MH 500 W, was used with a 3 kW power spindle, a maximum spindle speed of 4000 rpm, a feed rate of 3000 mm/min, and a total power of 11 kVA. A force

e-ISSN 2623-0313
p-ISSN 3032-1972

sensor with a maximum capacity of 15 kN was incorporated to measure axial compressive forces during FSW welding. To monitor the compressive force, the force sensor is connected to a digital display, as shown in Figure 5.

The clamping mechanism consists of the following components: clamps, clamping straps, and side straps, as shown in Figure 6. The clamping strap design allows a minimum 100 mm spacing between the clamp straps, allowing the welding tool to move freely without contacting them. The adjustable clamps enable 150 mm FSW tools to be used without the tool holder contacting the clamps. The side clamps are designed to stop the separation of the plates during the welding process, as this will adversely affect the quality of weld joints.

MECHANICAL TESTING

After the FSW process, the welded plates are kept at room temperature for a week to stabilize the plate structure. The specimens were then cut from each welded plate according to the American Society for Testing and Materials [21]. Figure 7 shows the FSW specimen and its dimensions.

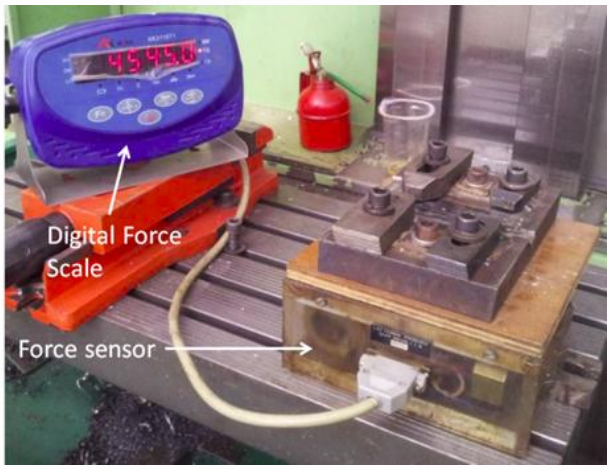

Figure 5. Force sensor and digital display connection

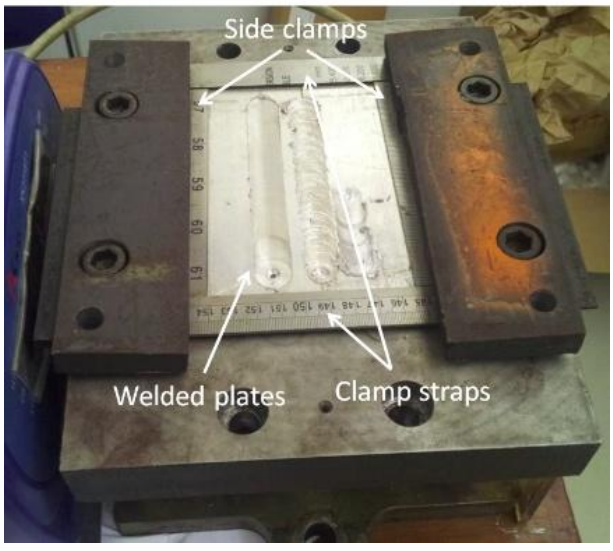

Figure 6. The FSW clamping mechanism

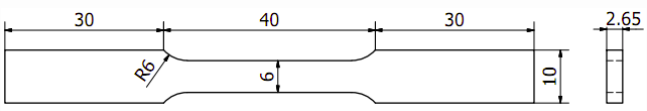

Figure 7. The FSW specimen and its dimensions

e-ISSN 2623-0313
p-ISSN 3032-1972

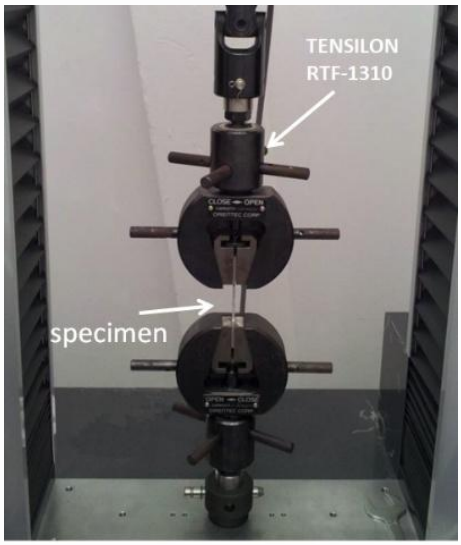

Figure 8. The tensile strength of the specimen is measured using UTTM TENSILON RTF-1310

Figure 9. Optical Microscope Nikon's Eclipse MA100

Tensile strength tests of the specimens were carried out using the Universal Tensile Testing Machine (UTTM) TENSILON RTF-1310 at room temperature, as shown in Figure 8. The crosshead speed of 0.5 mm/min was used to test the specimens. The average tensile strength results for each welded plate are then used to develop a relationship for FSW welding parameters.

MICRO-STRUCTURAL INVESTIGATION

The specimens for microstructural investigation were cut from the AA1100 friction stir-welded plates to the required dimensions using an EDM machine. The specimens were processed through four different stages [22]. Microstructural investigations were carried out using an optical microscope (Nikon's Eclipse MA100) in conjunction with an image analysis software Dino Capture 2.0 as shown in Figure 9.

EXPERIMENT RESULTS AND ANALYSIS

FSW process parameters significantly affect the mechanical properties of the friction-welded material. The parameters should be optimized to avoid degradation of the welded material's properties. The recommended technique for designing experiments is the Response Surface Methodology (RSM), which was developed by Box and Wilson [23]. RSM also measures the relationship between the controllable input parameters and the obtained response surfaces [9].

Development of the Experimental Design Matrix

Typical experimental design methods, such as full factorial, factorial, and CCRD (Central Composite Rotatable Design), are commonly used for process modeling. CCRD, developed by Box and Wilson [20], requires fewer experiments than the full or partial

e-ISSN 2623-0313
p-ISSN 3032-1972

factorial designs. This study uses a CCRD matrix with 20 sets of experimental runs, three selected independent welding parameters (tool rotational speed, welding speed, and tool axial force), and five levels. The total set of runs is selected using the equation. 1:

$$n = 2^k + 2k + m \quad (1)$$

where k = 3 is the independent welding parameter and m is the center point. In this study, m was chosen to be 6 (six), and the five levels of the experiment were ($\pm a$, ± 1, 0), where $a = 2^{k/4}$. The matrix design of this study is presented in Table 6.

.

The measured response parameter was the tensile strength. The experimental design created using Design Expert Software is presented in Table 7

Table 6. Coded values of parameters and tensile strength result

Parameters	Unit	Levels				
		-1.681	**-1**	**0**	**1**	**1.681**
Rotational speed (*N*)	RPM	700	800	900	1000	1100
Welding speeds (*S*)	mm/min	60	80	100	120	140
Axial force (*F*)	kN	2	3	4	5	6

Table 7. Classification of coded and actual values of FSW parameters

No	Coded Value of Parameters			Mechanical Properties	
				Tensile Strength (*TS*) (MPa)	
	N	***S***	***F***	**Experiment**	**Prediction**
1	-1	-1	-1	87	87
2	1	-1	-1	82	83
3	-1	1	-1	87	88
4	1	1	-1	85	86
5	-1	-1	1	89	90
6	1	-1	1	85	86
7	-1	1	1	89	90
8	1	1	1	86	88
9	-1.681	0	0	89	89
10	1.681	0	0	86	84
11	0	-1.681	0	84	84
12	0	1.681	0	89	87
13	0	0	-1.681	89	88
14	0	0	1.681	95	93
15	0	0	0	92	91
16	0	0	0	91	91
17	0	0	0	90	91
18	0	0	0	91	91
19	0	0	0	88	91
20	0	0	0	92	91

Mathematical Modeling

In this study, the mathematical relationship between FSW process parameters and weld ultimate tensile strength was investigated. The model developed is a second-order polynomial regression model that includes the main and interaction effects of all parameters. The response properties of the friction stir-welded joints are a function of rotational speed (N), welding speed (S), and axial force (F). The response surface can be expressed as Equation 2 [23]:

$$TS = f(N, S, F) \quad (2)$$

The equation of second-order polynomial regression used in this research to represent the response surface is given by Equation 3 (Mason et al., 2003):

e-ISSN 2623-0313
p-ISSN 3032-1972

$$Y = b_0 + \sum b_i x_i + \sum b_{ii} x_i^2 + \sum b_{ij} x_i x_j + e_r \quad (3)$$

where
b_0 is a constant value of response
b_i is a linear constant coefficient
b_{ii} is a quadratic constant coefficient
b_{ij} is an interaction constant coefficient
e_r is the error of the model

The values of those coefficients in Equation 3 were calculated using Equations 4 – 7 [8]. These model regression coefficients were calculated from the experimental data shown in Table 6.

$$b_0 = 0.165385(\sum Y) - 0.057692 \sum(X_i Y) \quad (4)$$
$$b_1 = 0.075 \sum(X_i Y) \quad (5)$$
$$b_{ii} = 0.070312 \sum(X_{ii} Y) + 0.005409 \sum(X_{ii} Y) - 0.057692 (\sum Y) \quad (6)$$
$$b_{ij} = 0.125 \sum(X_{ij} Y) \quad (7)$$

The equations of second-order polynomial regression, Equation 3, could then be expressed as Equation 8:

$$TS = b_0 + b_1(N) + b_2(S) + b_3(F) + b_{11}(N^2) + b_{22}(S^2) + b_{33}(F^2) + b_{12}(NS) + b_{13}(NF) + b_{23}(SF) \quad (8)$$

All the coefficients were tested for their significance at 95% confidence level, applying Fisher's F-test using Design Expert statistical software package.

To ensure the adequacy of the model, ANOVA (analysis of variance) analysis has been used. The analysis included tests for significance of the regression model and coefficients. The model was presented as a two-dimensional plot. Using the regression model in the Design Expert software, the analysis result, which shown in the summary Table 8, recommends the highest order of polynomial where the addition terms are significant. The equation of the developed mathematical model is given in Equation 9 below:

$$TS = 90.74 - 1.39N + 0.91S + 1.32F - 1.61N^2 - 1.96S^2 - 0.01F^2 + 0.5NS - 0.25SF \quad (9)$$

The adequacy of the developed models is then tested using ANOVA. The results of the ANOVA analysis are given in Table 8. It shows that the common criterion of the mathematical model is adequate and significant.

- With a 95% confidence level, *the Fratio (Fisher) ratio of the ANOVA analysis in Table 8, which equals* 4.59, is larger than the cumulative probabilities, 3.02. This criterion shows that the developed mathematical model is adequate.
- The significance value is found to be 0.013, which is lower than the upper limit, 0.05. If the significance value exceeds the upper limit, the model is insignificant.
- The adequate precision for measuring the signal-to-noise ratio is 7.52, which indicates that the model has an adequate signal. The ratio of adequate precision greater than 4 is desirable, therefore the model can be used to navigate the design space.
- Another criterion that is commonly used to illustrate the adequacy of a fitted regression model is the coefficient of determination (R^2). If R2 is 1.0, the predicted values from the mathematical model will exactly match the experimental values. The higher R2 values indicate that the regression model is adequate and can predict responses (Tensile Strength) without considerable error. For the developed model, the calculated R^2 values and adjusted R^2 values are above 81% and 63%, respectively. These values indicate that the regression models are significant.

e-ISSN 2623-0313
p-ISSN 3032-1972

Table 8. ANOVA Analysis Results

Regression Statistics	
Multiple *R*	0.90
R square	0.81
Adjusted *R* Square	0.63
Standard Error	1.91
Adequate Precision	7.52
Observations	20
Regression (Model)	
Degree of Freedom	9
Sum Square	149.89
Mean Square	16.65
F_{ratio}	4.59
Significance (Prob>F)	0.013
Residual (Error)	
Degree of Freedom	10
Sum Square	36.31
Mean Square	3.63
Total	
Degree of Freedom	19
Sum Square	186.20
Model	Significant

From F table, F(9,10, 0.05) = 3.02 < F = 4.59

The observed response (tensile strength) of friction-stir-welded AA1100 alloys, along with the model-predicted responses and their respective correlation graphs, is presented in Figure 10. The value of 'R2' for the above developed relationships is found to be 81%, which indicates a high correlation between experimental and predicted values along a trend line within the limits of the FSW process parameters.

Effect of FSW Process Parameters on Tensile Strength

The Pareto bar chart in Figure 11 shows the effective coefficients of FSW process parameters to the tensile strength of the predicted models. According to the chart, the second-order coefficient of S2 (square of welding speed) has the greatest effect on the tensile test, while the interaction coefficient of NF (rotational speed and axial force) is the least effective parameter in the model.

The graph in Figure 12 shows that the rotational speed, welding speed, and axial force have essential roles in the predicted model (tensile strength) when each FSW parameter moves from the center point, while other parameters are kept constant at the center point.

Figures 13, 14 and 15 present the effects of rotational speed and axial force on predicted tensile strength in line plot, contour plot and 3D surface, respectively. As the welding speed and the axial force are kept at constant values in Figure 5.4a, the rotational speeds that vary from lower to higher values change the tensile strength.

Figure 13. Effect of rotational speed (N) and axial force (F) on predicted tensile strength (TS). As the axial force is increased from F=2 kN to F=6 kN while the rotational and welding speeds are kept constant in the center point, the tensile strength of the mathematical model increases to TS = 93 MPa.

Figure 14. Effect of rotational speed (N) and axial force (F) on predicted tensile strength in a contour plot. The maximum tensile strength of 89.98 MPa has been found between the rotational speed of 800 rpm and 900 rpm, and the welding speed between 100 mm/min and 120 mm/min. The minimum tensile strength of 82.78 MPa is observed when the rotational and welding speeds are very close to 1000 rpm and 80 mm/min, respectively.

e-ISSN 2623-0313
p-ISSN 3032-1972

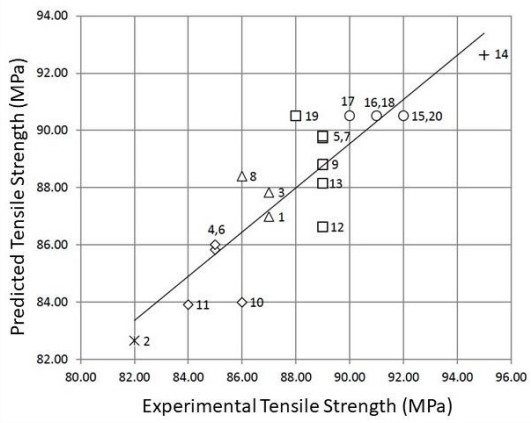

Figure 10. Comparison of actual and predicted tensile strength (Table 7).

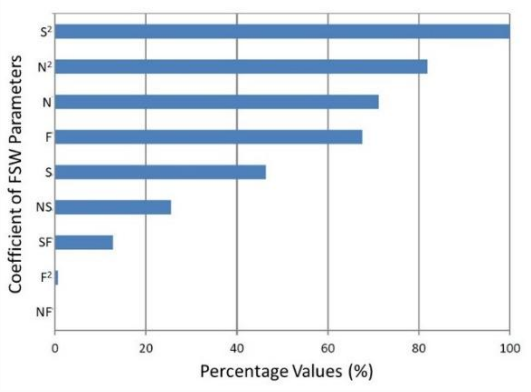

Figure 11. Factors affected FSW Parameters

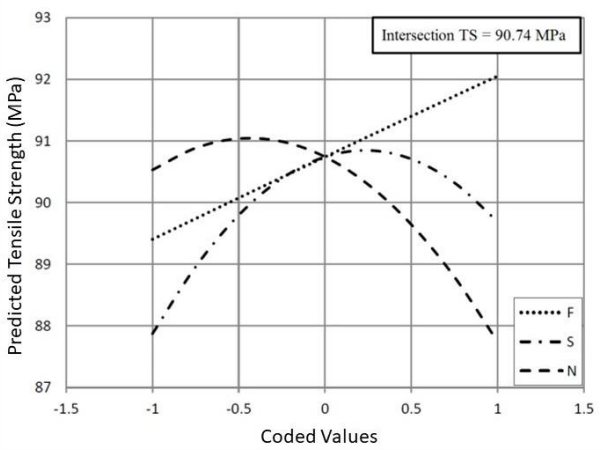

Figure 12. Effect of all FSW parameters on tensile strength of the predicted model. The intersection of the three parameters occurred at TS = 90.74 MPa.

e-ISSN 2623-0313
p-ISSN 3032-1972

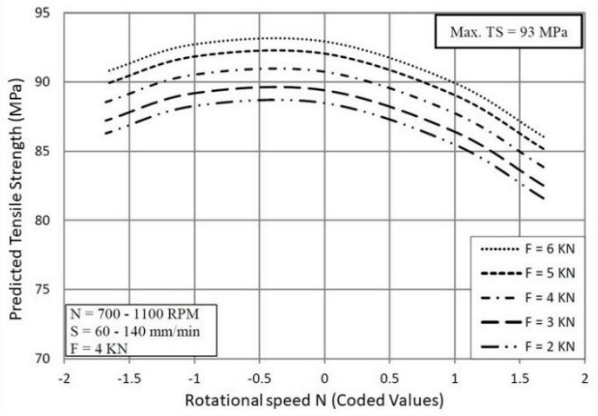

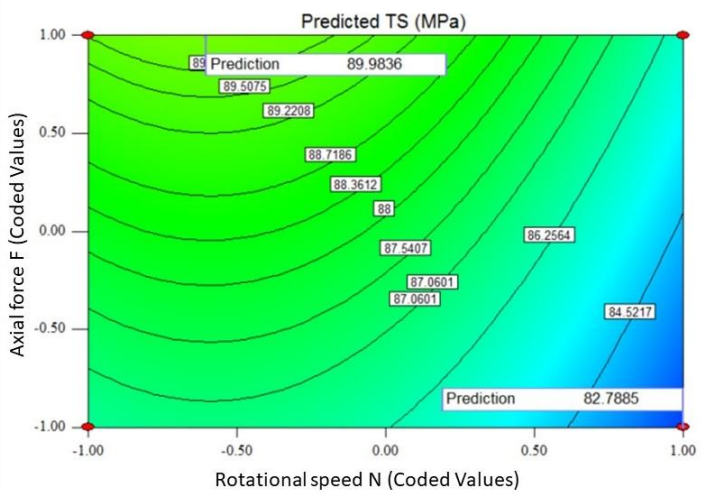

When reducing the rotational speed to its lowest level while keeping the welding speed and axial force at their center values, the tensile strength decreases. This is the result of the insufficient heat.

When increasing the rotational speed to a higher value while other parameters are kept constant, the tensile strength reaches the optimum values (93 MPa with the rotational speed of 900 rpm, welding speed of 100 mm/min, and axial force of 6 kN) as a result of sufficient heat for welding the FSW workpiece. The values of tensile strength fall to the minimum values when the rotational speed increases to the highest level. This increase in rotational speed will cause overheating at the weld joint, destroying the material's plastic structure.

In Figures 14 and 15, the maximum tensile strength of 89.98 MPa has been found between the rotational speed of 800 rpm and 900 rpm, and axial force, which is very close to 5 kN. The minimum tensile strength of 82.78 MPa is observed when the rotational speed and axial force are very close to 1000 rpm and 3 kN, respectively. In Figure 15, the optimization did not achieve the optimal tensile strength, even though the axial force had reached its maximum.

Figures 16, 17, and 18 show the effects of rotational and welding speeds on predicted tensile strength in line plots, contour plots, and 3D surfaces, respectively. Figure 16 shows that the welding speed has a significant effect on tensile strength, while the other two parameters are held constant at the center point. As the welding speed is at its lowest, the tensile strength is also at its lowest. The lowest tensile strength is due to a too-slow welding speed, which allows the heat generated by the rotational speed and axial force to melt the material.

e-ISSN 2623-0313
p-ISSN 3032-1972

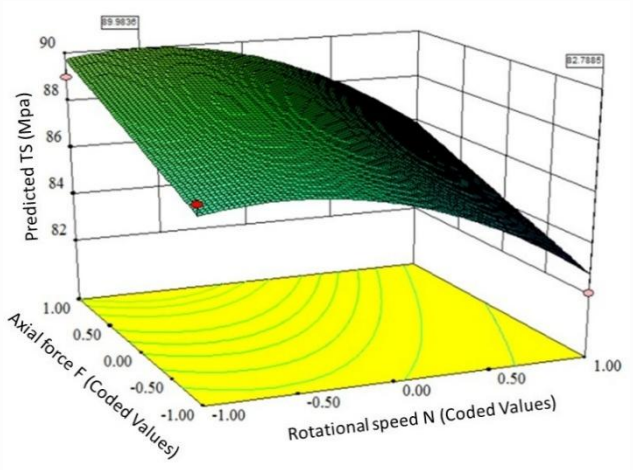

Figure 15. Effect of rotational speed (N) and axial force (F) on predicted tensile strength in 3D surface.

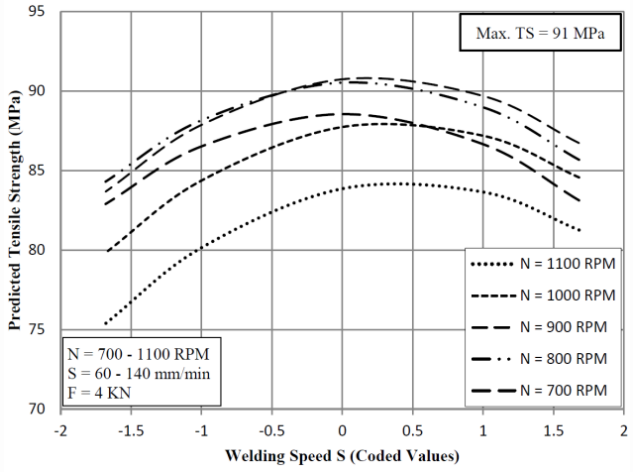

Figure 16. Effect of welding speed (S) and rotational speed (N) on predicted tensile strength.

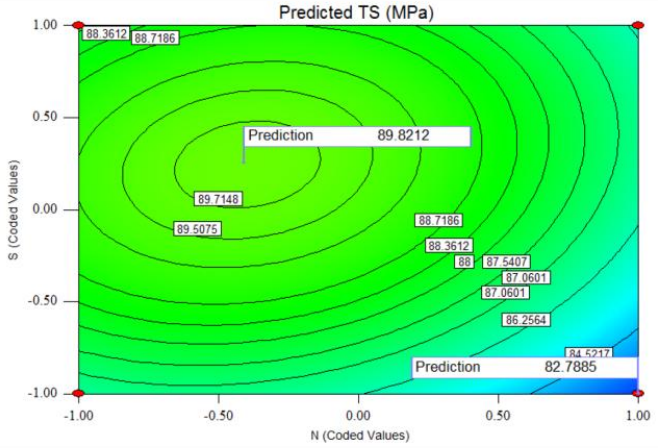

Figure 17. Effect of welding speed (S) and rotational speed (N) on predicted tensile strength in a contour plot.

e-ISSN 2623-0313
p-ISSN 3032-1972

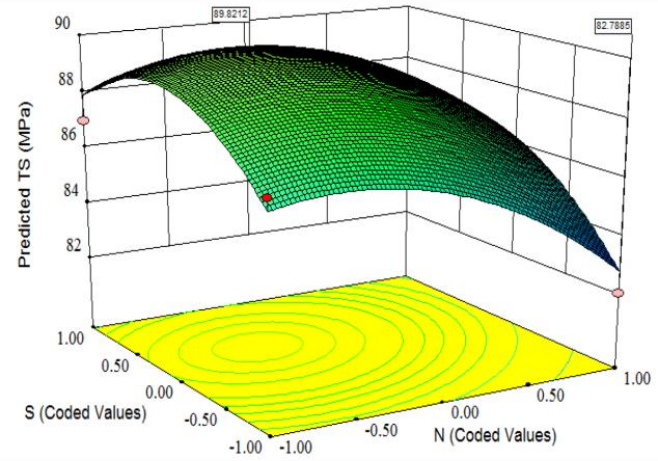

Figure 18. Effect of welding speed (S) and rotational speed (N) on predicted tensile strength in 3D surface

Increasing the welding speed to higher level will generate sufficient heat to soften the welding material that leads to the maximum tensile strength (91 MPa at the rotational speed of 900 rpm, welding speed of 100 mm/min, and axial force of 4 kN). As the welding speed rises above the highest point the FSW welding process could not create enough heat at 120 mm/min welding speed to weld the workpiece, resulting in dropping its tensile strength due to insufficient heat. In Figures 17 and 18, the maximum tensile strength of 89.82 MPa has been found between the rotational speed of 800 rpm and 900 rpm, and the welding speed between 100 mm/min and 120 mm/min. The lowest tensile strength of 82.78 MPa is observed during rotation speed and welding speed of each approaching 1000 rpm and 80 mm/min, respectively.

Figures 19, 20, and 21 indicate the effects of axial force and welding speed on predicted tensile strength in line plot, contour plot and 3D surface, respectively. Figure 19 shows that the axial force is a significant parameter for varying the tensile strength of the model while the other two parameters, rotational speed and welding speed, are kept constant in the center point. Low axial forces are insufficient to generate heat resulting in low tensile strength. As the axial force is increased above the center point, the FSW tool generates enough heat to weld the workpiece resulting in higher tensile strength. As the axial force is increased to the highest level, F = 6 kN, the tensile strength of the mathematical model reaches to the maximum point of 93 MPa while rotational and welding speed are kept constant in the center point. It shows that at this axial force level the heat is sufficiently generated for the optimum tensile strength. In Figures 19 and 20, the maximum tensile strength of 89.22 MPa has been found between the welding speed of 100 mm/min and 120 mm/min, and the axial force which is close to 5 kN, while the minimum tensile strength of 82.78 MPa is observed when the welding speed and axial force are very close to 80 mm/min and 3 kN respectively. In the case of Figure 21 is not different from the case of Figure 15, the optimization did not reach the optimized axial force which showed that in the axial force axis, the tensile strength keeps increasing even though the axial force reached the maximum point.

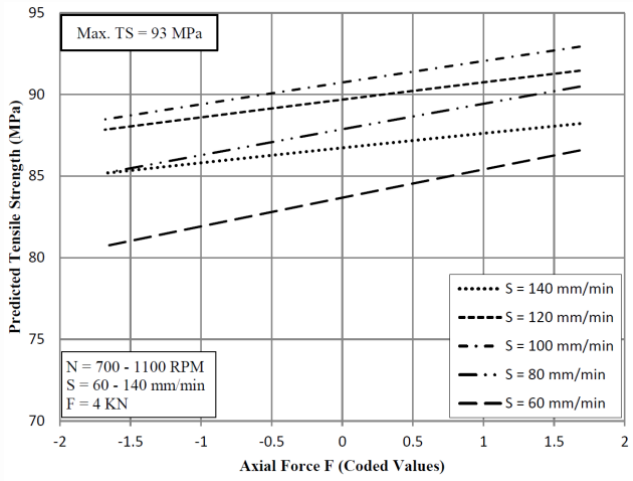

Figure 19. Effect of axial force (F) and rotational speed (N) on predicted tensile strength

e-ISSN 2623-0313
p-ISSN 3032-1972

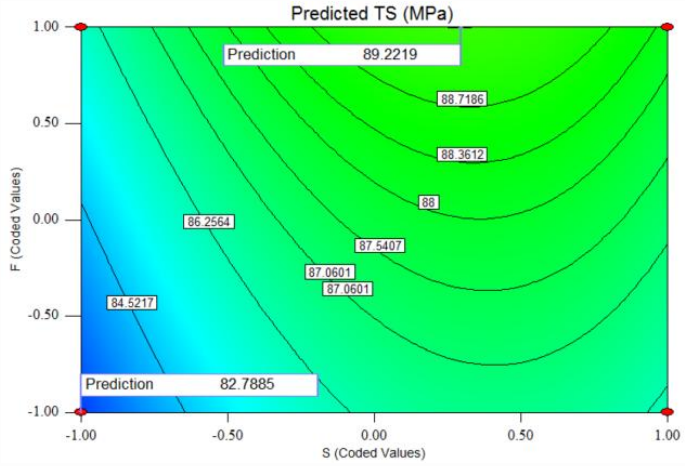

Figure 20. Effect of axial force (F) and welding speed (S) on predicted tensile strength in Contour plot.

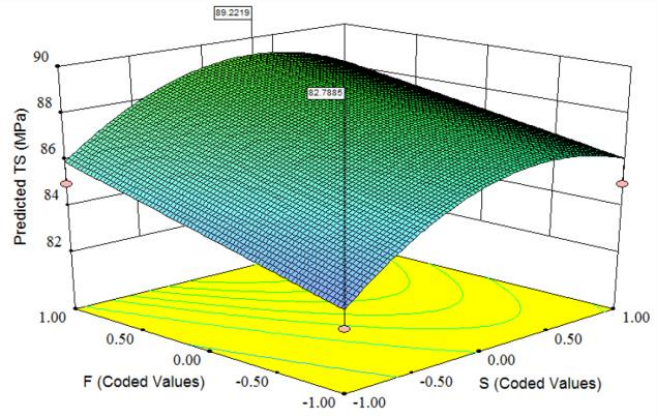

Figure 21. Effect of axial force (F) and welding speed (S) on predicted tensile strength in 3D surface

MACRO AND MICRO-STRUCTURAL INVESTIGATION

Macro and micro-structures of the cross-sectional welded joint have been investigated for different parameters. Figures 22 to 24 illustrate the macro and micro-structure in various FSW welding parameters. Advancing size (AS) and retreating size (RS) are notified as the two different sizes on the welded metal. For base metal (BM), heat affected zone (HAZ), thermo-mechanically affected zone (TMAZ), and weld nugget (WN) illustrate four different zones after the welding. In the macro-structural investigation of all welded cross-sections, there are no effects, holes, or tunnels found in the welded cross-sections by using different process parameters.

In Figure 22(b), the fine grain size along the WN zone is much smaller than that in the HAZ and TMAZ zone. This difference illustrates that WN zone has better strength than HAZ and TMAZ zone. The breaks point of the tensile test specimens is remarkably observed in the HAZ and TMAZ zone. This explains that the FSW parameters of Figure 22 produced the minimum tensile strength of 83 MPa. In Figure 23(b) with the tensile strength of 89 MPa and Figure 24(b) the tensile strength of 91 MPa, the grain sizes of WN, HAZ, and TMAZ zones is about the same.

OPTIMIZATION OF PARAMETERS OF FSW

The aims of this investigation were to maximize the tensile strength of friction stir welded joints of AA 1100 and to find the optimum process parameters from the developed mathematical model. Using counter plots shown at Figure 13 and Table 7, the maximum obtained tensile strength is 93 MPa. Using design of the experiment software and counter plots to maximize the *Tensile Strength* of welded joints, the obtained optimum operation parameters of the FSW are $N = 900$ rpm, $S = 100$ mm/min and $F = 6$ kN for a hexagon-shaped tool as shown in Figure 4.

e-ISSN 2623-0313
p-ISSN 3032-1972

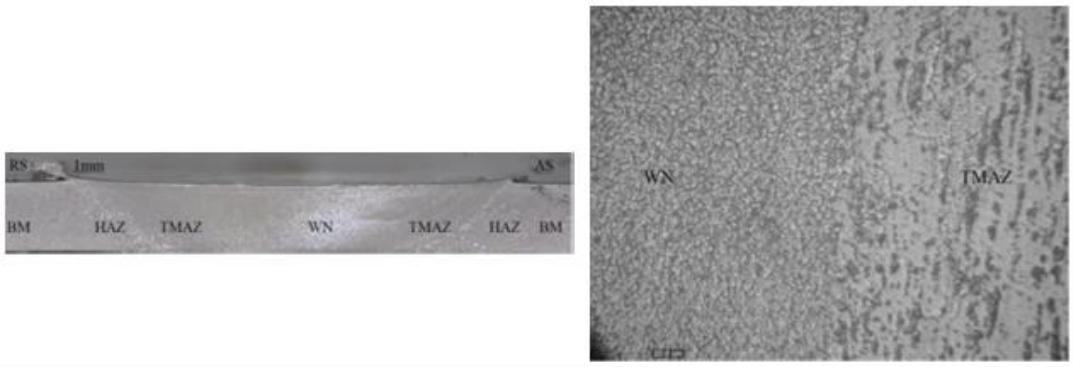

(a) (b)

Figure 22 (a) Macro structural, (b) Micro Structural, at Rotational speed N = 1000 rpm, welding speed S = 80 mm/min, and axial force F = 3 kN with the tensile strength equals 83 MPa which is the lowest value.

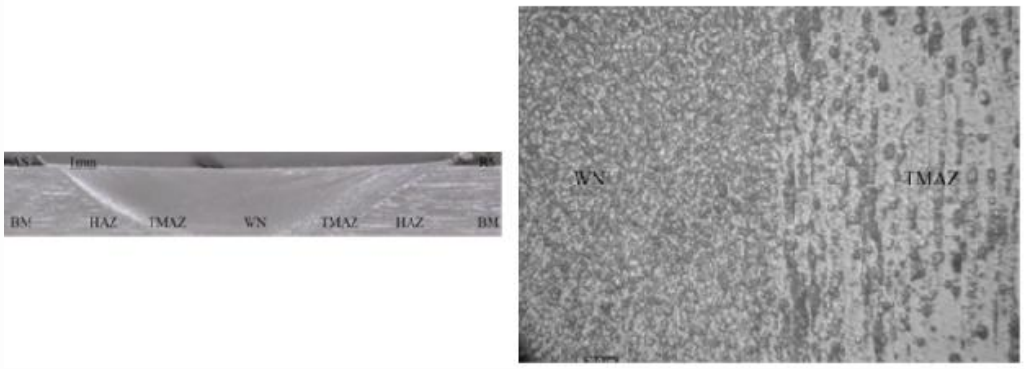

(b) (b)

Figure 23. (a) Macro structural, (b) Micro Structural, at Rotational speed N = 700 rpm, welding speed S = 100 mm/min, and axial force F = 4 kN with the tensile strength equals to 89 MPa.

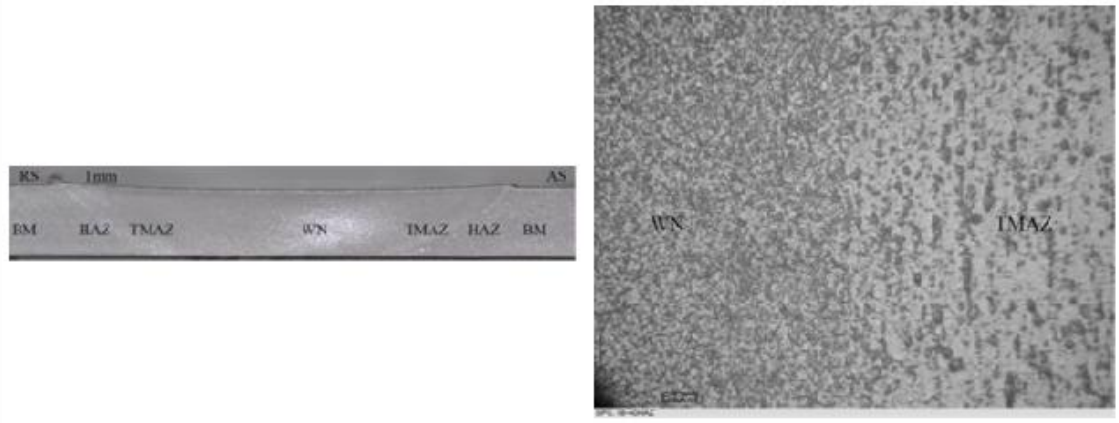

(a) (b)

Figure 24. (a) Macro structural, (b) Micro Structural, at Rotational speed N = 1000 rpm, welding speed S = 100 mm/min, and axial force F = 4 kN with the tensile strength equal to 91 MPa.

CONCLUSION

This paper presents an investigation into the process modeling of friction stir welding of AA1100 aluminum alloy using a hexagon-shaped tool to optimize the welding process parameters. The process parameters are optimized using Response Surface Methodology based on a central composite rotatable design with three parameters, five levels, and 20 runs. RSM based on a central composite rotatable design was successfully used to develop a mathematical model predicting the tensile strength of AA 1100 joints. The analysis showed that the developed model can be effectively used to predict joint tensile strength at the 95% confidence level. Tensile strength of the friction stir welded joints increased with the increase of tool

e-ISSN 2623-0313
p-ISSN 3032-1972

rotational speed, welding speed, and tool axial force up to a maximum value, and then decreased. Micro-structure of the weld nugget zone indicated that the friction stir welded plates contain a fine grain structure compared to the base metal, and this led to the high tensile strength of the welded material along the weld nugget zone.

REFERENCES

[1] W. M. Thomas, E. D. Nicholas, J. C. Needham, P. Temple-Smith, and C. J. Dawes, "Improvements to Friction Welding," Patent GB Patent No. 0615480, International patent application No. PCT/GB92/02203, 1991

[2] D. Lohwasser and Z. Chen, *Friction stir welding*. Cambridge CB21 6AH, UK: Woodhead Publishing Limited, 2010. doi: 10.1533/9781845697716.

[3] F. Lambiase, H. A. Derazkola, and A. Simchi, "Friction Stir Welding and Friction Spot Stir Welding Processes of Polymers—State of the Art," *Materials*, vol. 13, no. 10, p. 2291, May 2020, doi: 10.3390/ma13102291.

[4] Y. Ai, X. Shao, P. Jiang, P. Li, Y. Liu, and W. Liu, "Welded joints integrity analysis and optimization for fiber laser welding of dissimilar materials," *Opt Lasers Eng*, vol. 86, pp. 62–74, Nov. 2016, doi: 10.1016/j.optlaseng.2016.05.011.

[5] E. T. Akinlabi and S. A. Akinlabi, "Friction Stir Welding Process: A Green Technology," *International Journal of Mechanical and Mechatronics Engineering*, vol. 6, no. 11, pp. 2514–2515, 2012.

[6] A. Shrivastava, M. Krones, and F. E. Pfefferkorn, "Comparison of energy consumption and environmental impact of friction stir welding and gas metal arc welding for aluminum," *CIRP J Manuf Sci Technol*, vol. 9, pp. 159–168, May 2015, doi: 10.1016/j.cirpj.2014.10.001.

[7] C. Vimalraj and P. Kah, "Experimental Review on Friction Stir Welding of Aluminium Alloys with Nanoparticles," *Metals (Basel)*, vol. 11, no. 3, p. 390, Feb. 2021, doi: 10.3390/met11030390.

[8] S. Rajakumar and V. Balasubramanian, "Establishing relationships between mechanical properties of aluminium alloys and optimised friction stir welding process parameters," *Mater Des*, vol. 40, pp. 17–35, Sep. 2012, doi: 10.1016/j.matdes.2012.02.054.

[9] A. Heidarzadeh, H. Khodaverdizadeh, A. Mahmoudi, and E. Nazari, "Tensile behavior of friction stir welded AA 6061-T4 aluminum alloy joints," *Mater Des*, vol. 37, pp. 166–173, May 2012, doi: 10.1016/j.matdes.2011.12.022.

[10] A. Razal Rose, K. Manisekar, V. Balasubramanian, and S. Rajakumar, "Prediction and optimization of pulsed current tungsten inert gas welding parameters to attain maximum tensile strength in AZ61A magnesium alloy," *Mater Des*, vol. 37, pp. 334–348, May 2012, doi: 10.1016/j.matdes.2012.01.007.

[11] R. Paventhan, P. R. LAKSHMINARAYANAN, and V. BALASUBRAMANIAN, "Prediction and optimization of friction welding parameters for joining aluminium alloy and stainless steel," *Transactions of Nonferrous Metals Society of China*, vol. 21, no. 7, pp. 1480–1485, Jul. 2011, doi: 10.1016/S1003-6326(11)60884-4.

[12] L. De Filippis, L. Serio, D. Palumbo, R. De Finis, and U. Galietti, "Optimization and Characterization of the Friction Stir Welded Sheets of AA 5754-H111: Monitoring of the Quality of Joints with Thermographic Techniques," *Materials*, vol. 10, no. 10, p. 1165, Oct. 2017, doi: 10.3390/ma10101165.

[13] L. Cederqvist and A. Reynolds, "Factors affecting the properties of friction stir welded aluminum lap joints," *American Welding Society*, vol. 80, no. 12, pp. 281–287, 2001.

[14] J. A. Arbegast, "Hot Deformation of Aluminium Alloys III," The Minerals, Metals & Materials Society, 2003, pp. 313–327.

[15] R. S. Mishra and Z. Y. Ma, "Friction stir welding and processing," *Materials Science and Engineering: R: Reports*, vol. 50, no. 1–2, pp. 1–78, Aug. 2005, doi: 10.1016/j.mser.2005.07.001.

[16] P. A. Colegrove and H. R. Shercliff, "CFD modelling of friction stir welding of thick plate 7449 aluminium alloy," *Science and Technology of Welding and Joining*, vol. 11, no. 4, pp. 429–441, Jul. 2006, doi: 10.1179/174329306X107700.

[17] K. J. Colligan and R. S. Mishra, "A conceptual model for the process variables related to heat generation in friction stir welding of aluminum," *Scr Mater*, vol. 58, no. 5, pp. 327–331, Mar. 2008, doi: 10.1016/j.scriptamat.2007.10.015.

[18] P. A. Colegrove, H. R. Shercliff, and R. Zettler, "AModel for Predicting the Heat Generation and Temperature in Friction Stir Welding from the Material Properties," *Science and Technology of Welding & Joining*, vol. 12, no. 4, pp. 284–297, 2007.

e-ISSN 2623-0313
p-ISSN 3032-1972

[19] ASTM B 209M – 07, *Standard Specification for Aluminum and Aluminum-Alloy Sheet and Plate (Metric)*. ASTM International, 2007.

[20] ASTM A 600 – 92a, *Standard Specification for Tool Steel High Speed*. ASTM International, 2005.

[21] ASTM E8/E8M – 11, *Standard Test Methods for Tension Testing of Metallic Materials*. ASTM International, 2012.

[22] M. R. Louthan, *Optical Metallography*. ASM Handbook, 1986.

[23] R. L. Mason, R. F. Gunst, and J. L. Hess, *Statistical Design and Analysis of Experiments*. Hoboken, New Jersey: John Wiley & Sons, Inc., 2003.